

Exploration on pressure-induced phase transition of cerium mononitride from first-principles calculations

Meiguang Zhang, Haiyan Yan, Qun Wei, and Hui Wang

Citation: *Appl. Phys. Lett.* **102**, 231901 (2013); doi: 10.1063/1.4809921

View online: <http://dx.doi.org/10.1063/1.4809921>

View Table of Contents: <http://apl.aip.org/resource/1/APPLAB/v102/i23>

Published by the [American Institute of Physics](#).

Additional information on *Appl. Phys. Lett.*

Journal Homepage: <http://apl.aip.org/>

Journal Information: http://apl.aip.org/about/about_the_journal

Top downloads: http://apl.aip.org/features/most_downloaded

Information for Authors: <http://apl.aip.org/authors>

ADVERTISEMENT

a sampling
of our
products



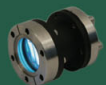
for surface
and materials
science

www.
rbdinstruments
.com

celebrating over
20 years
of innovation



deposition
tools



desorption
systems



sputter
ion sources



viewports



usb
picoammeters

Exploration on pressure-induced phase transition of cerium mononitride from first-principles calculations

Meiguang Zhang,^{1,a)} Haiyan Yan,² Qun Wei,^{3,a)} and Hui Wang⁴

¹Department of Physics and Information Technology, Baoji University of Arts and Sciences, Baoji 721016, China

²College of Chemistry and Chemical Engineering, Baoji University of Arts and Sciences, Baoji 721013, China

³School of Science, Xidian University, Xi'an 710071, China

⁴National Laboratory of Superhard Materials, Jilin University, Changchun 130012, China

(Received 18 March 2013; accepted 24 May 2013; published online 10 June 2013)

Recently, pressure-induced phase transition of CeN from ambient *B1* phase to the *B2* phase has been experimentally reported at the pressure of 65–70 GPa. Nevertheless, the full transformation of the high-pressure *B2* phase has not been observed in the experiment as the authors said. Here we predict an unexpected anti-*B10* high-pressure phase which is energetically more preferable than the *B2* phase at the studied pressure range, disproving the experimental result. Our argument has been supported by the softening of both elastic constant C_{44} in *B1* phase and transverse acoustic mode at the zone boundary M point of *B2* phase. © 2013 AIP Publishing LLC.
<http://dx.doi.org/10.1063/1.4809921>

Rare-earth (RE) mononitrides have received much attention due to their unfilled and highly localized *4f* electrons. As a function of their chemical environment, these compounds display an extraordinarily wide range of electronic, magnetic, optical, and magneto-optical properties with, among other things, potential practical applications in the field of spintronics.^{1,2} One of promising compounds, CeN, is the first member of the series of rare-earth mononitrides, which all crystallize in the NaCl structure (hereafter denoted as *B1*).^{3,4} In the *B1* phase, CeN is likely to contain Ce³⁺ and N³⁻ ions. It is, however, a conductor. This leads to the possibility of a crystal composition of the form Ce⁴⁺N³⁻e⁻, with one electron left in the conduction band. Meanwhile, the magnetic properties of CeN are those one would expect of a conductor: Pauli paramagnetism is observed, which is definitely out of the ordinary for a Ce³⁺ compound. On the contrary, the other Ce pnictides have shown more conventional behavior, that is, antiferromagnetic ordering of *4f* electrons remaining on each Ce.⁵ The reasons for the peculiar electronic and magnetic properties of CeN have been extensively debated in a considerable number of experimental and theoretical studies. The most prevalent two explanations for the localized versus itinerant magnetic properties of *4f* electrons in CeN are summarized as Kondo screened scenario and “band picture” in a recent work.⁶

As fascinating nitrides fuels, the thermodynamic properties of CeN have been studied both experimentally and theoretically in the past.^{6,7} Another interesting topic of research is the crystallographic transformations of CeN under high pressure. It seems as if the theoretical and experimental studies,^{5,8,9} have reached the consensus that CeN undergoes a structural phase transition from *B1* to CsCl phase (hereafter denoted as *B2*) at pressures of 62–88 GPa. Nevertheless, the full transformation of the high-pressure *B2* phase has not been observed in the recent experiment⁹ at higher pressure (77 GPa)

as the authors said. Meanwhile, this understanding is far from clear due to the absence of angle-dispersive X-ray diffraction patterns of CeN at different pressures. Accordingly, this question is open until convincing proof is provided. More recently, two stories of the high pressure phases for PrN and LaN, the family members of CeN, have been determined experimentally by Cynn *et al.*¹⁰ and Schneider *et al.*¹¹ These findings have confirmed that both PrN and LaN yield a phase transformation from the ground-state *B1* phase to a tetragonal structure (distorted *B2*-like structure, hereafter denoted as anti-*B10*) with ~8.8% and 11% volume collapses at ~40 GPa and ~26.5 GPa, respectively. These two experiments definitely ruled out the earlier belief of the *B1*→*B2* high-pressure phase transitions of PrN and LaN. Therefore, the exploration of the reasonable high pressure structure of CeN is still required.

In the present work, the crystal structure prediction is based on a global minimization of free-energy surfaces merging *ab initio* total energy calculations via particle swarm optimization (PSO) technique^{12,13} in the pressure range of 0–100 GPa with 1–4 formula units (f.u.) per simulation cell, as implemented in the Crystal structure ANALYSIS by Particle Swarm Optimization (CALYPSO) code.¹³ The density functional theory (DFT) calculations are carried out on the basis of the frozen-core projected augmented wave (PAW) method¹⁴ as implemented in the VASP code.¹⁵ The energy cutoff of 600 eV and appropriate Monkhorst-Pack *k* meshes¹⁶ are chosen to ensure that enthalpy calculations are well converged to better than 1 meV/atom. To deal with the strongly correlated *4f* states of Ce, the on-site Coulomb repulsion among the localized Ce *4f* electrons is described by using the local density approximation plus Coulomb interaction parameter (LDA+U) formalisms formulated by Dudarev *et al.*,^{17,18} where the double counting correction has already been included. Here the Coulomb *U* is treated as a variable, while the exchange energy is set to be a constant $J = 0.989$ eV, which is the same as in a previous study of CeN.¹⁹ And the quasi-harmonic Debye model²⁰ is applied to

^{a)} Authors to whom correspondence should be addressed. Electronic addresses: zhmgbj@126.com and weiaqun@163.com.

TABLE I. Calculated lattice constant a_0 , bulk modulus B_0 , and its pressure derivative B'_0 for ground-state B1-CeN by using the LDA, GGA, and LDA+U method, respectively. The available experimental values are also listed for comparison.

Method	a_0 (Å)	B_0 (GPa)	B'_0
Exp.	5.021(2) ^{a,b}	156(3) ^{a,c}	4.000 ^a
LDA	4.966	169.7	4.011
GGA	5.045	155.2	4.125
LDA+U (U=0)	4.942	180.2	3.637
LDA+U (U=1)	4.964	175.2	3.725
LDA+U (U=2)	4.987	170.2	3.846
LDA+U (U=3)	5.009	165.2	3.939
LDA+U (U=3.5)	5.019	163.0	3.960
LDA+U (U=4)	5.031	160.2	4.028
LDA+U (U=5)	5.052	155.1	4.154
LDA+U (U=6)	5.075	150.3	4.224

^aRef. 9.

^bRef. 22.

^cRef. 23.

investigate the thermodynamic properties of CeN. Single crystal elastic constants are determined from evaluation of the stress tensor generated small strain. Phonon calculations were performed using the small displacement method as implemented in the PHONOPY code.²¹

Table I lists the lattice constant (a_0), bulk modulus (B_0), and pressure derivative of the bulk modulus (B'_0) for the B1-CeN at ambient conditions, along with the available experimental values.^{9,22,23} The bulk moduli and its pressure derivative is obtained by fitting pressures and cell volumes with the third-order Birch-Murnaghan equation of state (EOS).²⁴ As can be seen, the predicted lattice parameter (bulk modulus) is smaller (larger) within LDA than that within generalized gradient approximation (GGA), features which are common for these two approaches. For the LDA+U approaches, the calculated a_0 in Table I improves upon the

pure LDA and GGA by steadily increasing its amplitude with U. Actually, at a typical value $U = 3.5$ eV, the LDA + U gives $a_0 = 5.019$ Å, which is very close to the experimental data of 5.021(2) Å.^{9,22} Meanwhile, the calculated bulk modulus of CeN is 163 GPa, which is slightly larger than that of experimental data (156(3) GPa).^{9,23} For $U = 5$ eV, the calculated lattice constant a_0 has a much larger deviation from the experimental data than that of $U = 3.5$ eV although the corresponding bulk modulus is well in agreement with the experimental value.²³ Overall, comparing the experimental data listed in Table I, the accuracy of our crystal structure prediction for CeN is made quite satisfactory by tuning the effective Hubbard parameter U at 3.5 eV within the LDA+U approaches, which supplies the safeguard for our following study of thermodynamic properties, mechanical properties, and pressure-induced phase transition of CeN.

In order to provide some insight into the temperature effects on CeN, the investigations on its structural and thermodynamic properties under high temperature are determined by the quasi-harmonic Debye model, in which the phononic effect is considered. The temperature acting on the system as a function of the lattice parameter is plotted in Fig. 1(a), together with experimental data.^{3,7,25,26} Strikingly, the results obtained by LDA+U sit perfectly between curves representing pure GGA and LDA calculations and are close to these experimental data at the temperature range of 0–600 K. This result confirms that on-site Coulomb interaction is dominating the problem at the elevated temperature. However, at higher temperature (>600 K), the experimental data show a somewhat unusual behavior, with a quick increase in lattice constants that cannot be well described by the LDA+U approach. This result may be due to a temperature-driven transition into a trivalent state of the Ce ions.⁶ The calculated heat capacities at constant pressure C_P and constant volume C_V with the temperature of CeN at ambient pressure are shown in Fig. 1(b), together with the

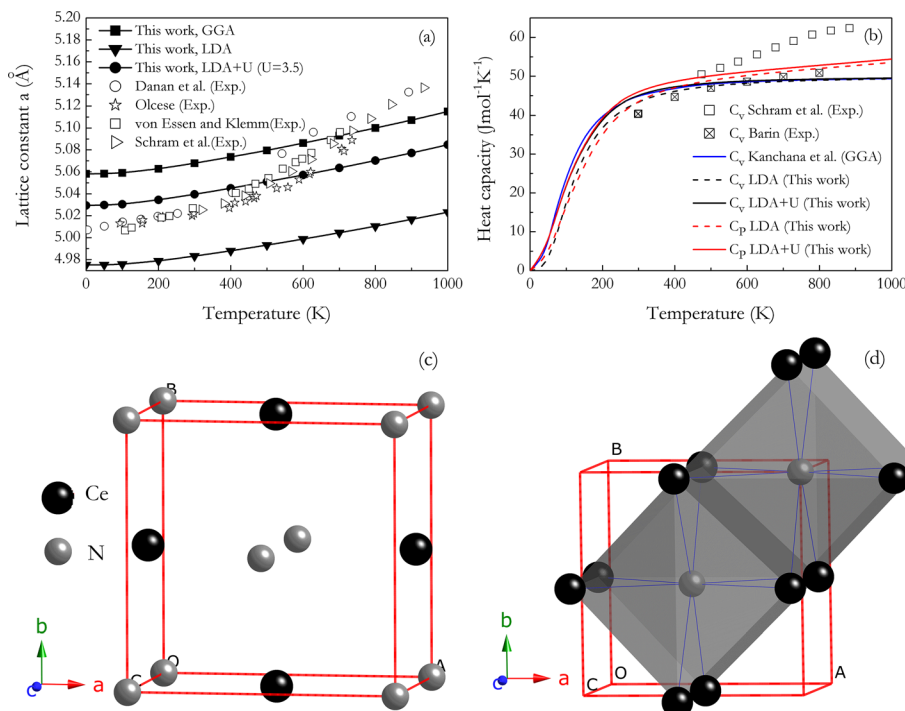


FIG. 1. Lattice parameters (a) and heat capacities C_V and C_P (b) of B1-CeN at various temperatures and ambient pressures. For comparison, previous experimental data and theoretical values are also shown. Crystal structure of anti-B10 phase (c) and polyhedral views of the anti-B10 phase (d) for CeN.

experimental data^{7,27} and other theoretical results.⁶ The difference between C_P and C_V is very small at low temperatures. However, at high temperatures, C_P increases uniformly with increments of the temperature, and the C_V approaches a constant value, which reaches the Dulong-Petit limit at sufficiently high temperatures when the anharmonic effect is suppressed. The LDA+U results for C_V sit perfectly and again between curves representing LDA and GGA results⁶ at the temperature range of 0–600 K. Meanwhile, these LDA+U results are in agreement with the available experimental data reported by Barin²⁷ for the temperature range of 300–800 K. Accordingly, we suppose that the localized picture anticipated in the LDA+U appears to be well suited for CeN at high temperatures. Third, in contrast the experimental data points⁷ are higher than the calculated C_V at higher temperature $T > 800$ K, which shows that additional entropy is stored in the system. This could be due to anharmonic effects, possibly combined with the formation of disordered local moments as suggested by Kanchana *et al.*⁶ Besides, we suppose that this might be due to the temperature-driven transition of the valent state of the Ce ions that resembles the high pressure behaviors of the lattice parameter mentioned above.

The excellent agreement between the calculated structural and thermodynamic results and available experimental data for the ground-state $B1$ phase gives us confidence to further explore the possible high-pressure phases for CeN. At 5 GPa and 25 GPa, our simulations, with the only input being the chemical composition of Ce:N = 1:1, predicted the most stable structure to be the experimental $B1$ phase, validating our PSO method adopted here. For higher pressures at 50 GPa and 100 GPa, a distorted $B2$ -like structure: the anti- $B10$ phase [Fig. 1(c)] was uncovered. This tetragonal structure is isostructural to the high-pressure phases of PrN and LaN, which have been confirmed in the recent experimental works.^{10,11} The anti- $B10$ phase contains two CeN f.u. in a unit cell ($a = b = 3.943$ Å and $c = 2.840$ Å at 50 GPa within LDA+U), in which two inequivalent atoms, N and Ce,

occupy the Wyckoff $2a$ (0, 0, 0) and $2c$ (0, 0.5, 0.420) sites, respectively. In more detail, this anti- $B10$ phase consists of a fundamental building block [Fig. 1(d)]: a polyhedron with one N atom at the centre and eight Ce atoms at the corners, meaning each N atom has eight nearest neighbors. This polyhedron can also be viewed as a distorted $B2$ -like structure. It is known that a stable crystalline structure requires all phonon frequencies to be positive. We have thus calculated the phonon dispersion curves of the anti- $B10$ phase at 80 GPa as shown in Fig. 2(c). No imaginary phonon frequencies are found in the whole Brillouin zone, indicating the dynamic stability of this high-pressure phase.

To determine the phase transition pressure, we have plotted out the enthalpy curves of the anti- $B10$ phase relative to the ambient-pressure $B1$ phase in the LDA+U framework in Fig. 2(a), along with the previously reported $B2$ phase for comparison. The equation of states, calculated by fitting the total energy vs volume data into the third-order Birch-Murnaghan EOS,²⁴ is shown in Fig. 2(b). These results suggest that the $B1 \rightarrow$ anti- $B10$ phase transition of CeN is first-order with clear volume drops of 12.2%, which will be easily detected in further experiments. In Fig. 2(a), it is confirmed that the predicted anti- $B10$ phase becomes more stable than the $B1$ phase above 37.5 GPa. However, the $B2$ phase possesses larger enthalpy values compared to those of the anti- $B10$ phase in the studied pressure range. The phase transition pressure from the $B1$ to $B2$ phase takes place at about 40 GPa as suggested by our enthalpy difference calculations (LDA + U). This value is lower than those previous theoretical values predicted by Svane *et al.*⁵ using the self interaction correction plus local spin density approximation (SIC-LSD) method ($B1 \rightarrow B2$, 62 GPa) and Rukmangad *et al.*⁸ using the Hartree-Fock method ($B1 \rightarrow B2$, 88 GPa). These differences may be attributed to the different theoretical methods applied in calculations. At this point one question is naturally raised regarding the predicted anti- $B10$ high pressure phase of CeN, which contradicts the experimentally reported $B2$ high pressure phase.⁹ Here we provide three

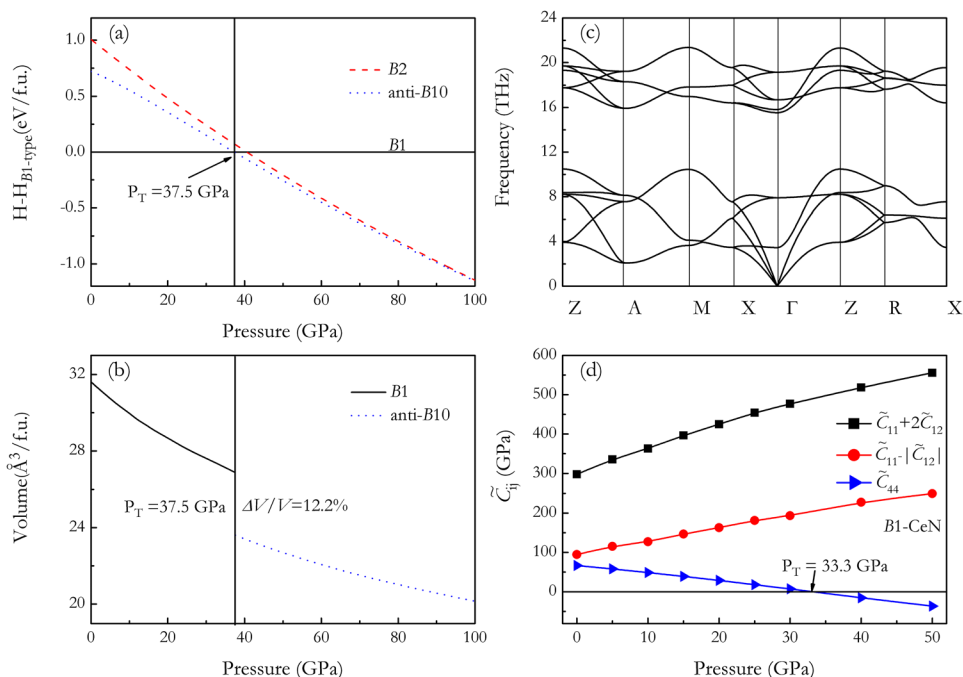


FIG. 2. Enthalpy of anti- $B10$ phase relative to the $B1$ phase as a function of pressure (a), the calculated volumes as a function of pressure for the anti- $B10$ phase and the $B1$ phase (b), phonon dispersion curves of the anti- $B10$ phase for CeN at 80 GPa (c), and calculated \tilde{C}_{44} , $\tilde{C}_{11} - |\tilde{C}_{12}|$, and $\tilde{C}_{11} + 2\tilde{C}_{12}$ under different isotropic pressures (d).

arguments to answer this question. First, our predicted anti-*B10* phase is indeed energetically more preferable than the *B2* phase in the pressure range of 0–100 GPa presented in Fig. 2(a). Second, we have calculated the phonon dispersion curves of the *B2* phase at 80 GPa in order to check the dynamic stability of CeN according to the phase transition pressure of *B1*→*B2* (>77 GPa) determined in this recent experimental work.⁹ In Fig. 3(a), it is clearly seen that the phonon spectrum shows a large imaginary frequency at M point, signaling the dynamic instability of the *B2* phase for CeN at high pressure. Thirdly, compared to two recent experimental works about the pressure-induced phase transitions of PrN and LaN mentioned above, the high pressure experiment of CeN⁹ did not give angle-dispersive X-ray diffraction patterns at different pressures. Only an energy-dispersive X-ray diffraction of CeN at a certain angle $\theta = 6.32^\circ$ is presented in their work, so one cannot see the full transformation to the *B2* phase at high pressure. Therefore, the *B2* phase cannot be definitively determined by this X-ray diffraction pattern. To further support our predictions, the phase transformation mechanism of *B1*→anti-*B10* of CeN has been fully explored in the underlying works.

The pressure dependence of elastic constants is a very important indicator of the mechanical stability of crystals at varying pressure. As is known, for a cubic crystal, the mechanical stability under isotropic pressure is judged from the following conditions:²⁸

$$\tilde{C}_{44} > 0, \tilde{C}_{11} - |\tilde{C}_{12}| > 0, \tilde{C}_{11} + 2\tilde{C}_{12} > 0,$$

where $\tilde{C}_{\alpha\alpha} = C_{\alpha\alpha} - P$ ($\alpha = 1$ and 4), $\tilde{C}_{12} = C_{12} + P$. Thus, we performed calculations on the pressure dependence of elastic constants for *B1*-CeN. As shown in Fig. 2(d), the values of $\tilde{C}_{11} - |\tilde{C}_{12}|$ and $\tilde{C}_{11} + 2\tilde{C}_{12}$ are all positive under pressure and increase uniformly with increments of the pressure. However, it should be noted that the \tilde{C}_{44} shows a softening trend and drops to zero at about 33.3 GPa. This result suggests that the *B1*-CeN is mechanically unstable when $P > 33.3$ GPa. Thus, we conclude that there must be a

structural phase transition occurring in the pressures according to relations of the mechanical stability under isotropic pressure, as suggested by Karki *et al.*²⁹ and Wang *et al.*³⁰ Note that this transition pressure (33.3 GPa) is consistent with the phase transition pressure of CeN from the *B1* to anti-*B10* phase obtained from equal enthalpies [Fig. 2(a)], indicating the accuracy of the predicted phase transition pressure of CeN. To understand phase transformation mechanism of CeN on a fundamental level, we have checked the lattice dynamic properties of the *B2* [Fig. 3(a)] phase at 80 GPa. In Fig. 3(a), it is clear that the transverse acoustic (TA) modes become notably softened at the M (0.5, 0.5, 0.0) point in the Brillouin zone boundary, indicating that CeN cannot stabilize in the *B2* phase at high pressure. It is known that a soft mode is intimately associated with symmetry-broken transformation of the structure and, as a consequence, a lower-symmetry child structure having a group-subgroup relation with the parent structure will be energetically favoured.^{31,32} A reasonable way to unveil the transformed phase is by a twofold procedure: freezing atoms along the eigenvector of the soft mode and then performing structural relaxations to release their internal stress. This technique has been applied to predictions of the high-pressure structures of ZnO,³¹ MgTe,³² and MgH₂.³³ In Fig. 3(b), we depict atomic vibrations along the eigenvector of the TA(M) mode, where N atoms stay relatively static while Ce atoms at the corners of two opposite planes in the *B2* cells move oppositely along the *c* axis of the crystal. We then calculate the total energies as a function of atomic displacements along the eigenvectors of the TA(M) mode at the selected pressure of 80 GPa, as shown in Fig. 3(c). The total energies are normalized to that of the *B2* phase for comparison. This predicted phase can be identified by the structural optimization with respect to the atomic distortions [about 0.05 *a* for CeN in Fig. 3(c)] where the energy minimum is formed. Strikingly, the resulting high-pressure phase is exactly the anti-*B10* phase, which corroborates our structural predictions by PSO simulations. Based on the current results, future experiments would be beneficial to clarify the existence of the anti-*B10* phase for CeN.

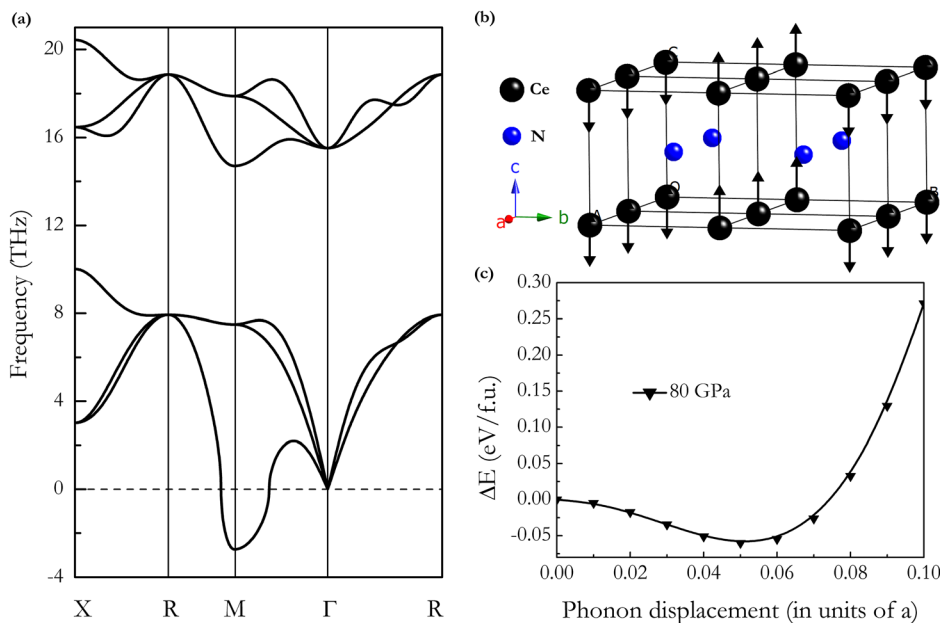


FIG. 3. Phonon dispersion curves of *B2* structure at 80 GPa (a). In the $2 \times 2 \times 1$ supercell of *B2* structure. Ce atomic distortion along the eigenvector of TA(M) mode as indicated by the arrows results in the formation of anti-*B10* structure (b). Total energies with atomic displacement along the eigenvectors of TA(M) mode at 80 GPa (c).

As shown in the Fig. 2(a), the enthalpy of the *B2* phase becomes competitive with anti-*B10* phase at pressures close to 100 GPa, which indicates that the potential associated to displacement of Ce atoms in the anti-*B10* structures [see Fig. 3(d)] gets smaller and more anharmonic with increasing pressure. It is expected that a lattice distortion of dynamical nature as the cubic cell undergoes large amplitude tetragonal fluctuations would be produced by increasing temperature or just by quantum fluctuations, and therefore, the *B2* as an "average" structure would be observed at a certain region of the phase diagram. A similar case has been reported for simple cubic structure of Ca at high pressures,³⁴ in which X-ray diffraction patterns associated with the dynamically distorted lattice plane show preferential broadening. Similarly, the dynamical nature of the lattice distortion of CeN at high pressures could also be identified by X-ray diffraction. That is, however, beyond the scope of this Letter.

In conclusion, the ground state properties as well as the high temperature and high pressure behavior of CeN were studied by using the first-principles method. By choosing the Hubbard *U* parameter at around 3.5 eV within the LDA+*U* approach, the lattice parameters and heat capacities were calculated for the ambient *B1* phase and the obtained results are shown to accord well with experiments. Furthermore, a pressure-induced phase transition from ambient *B1* to a tetragonal high pressure anti-*B10* phase of CeN has been predicted by using the particle swarm optimization technique, ruling out a long-held of the existence of *B2* high pressure. The phase transition mechanism of *B1*→anti-*B10* has fully clarified the mechanical instability of the *B1* phase and the softening TA phonon mode at the zone boundary M point of the *B2* phase.

This work was financially supported by the Natural Science Foundation of China (No. 11204007), Natural Science Basic Research plan in Shaanxi Province of China (Grant No. 2012JQ1005), Education Committee Natural Science Foundation in Shaanxi Province of China (Grant No. 2013JK0638), and the Fundamental Research Funds for the Central Universities.

¹S. A. Wolf, D. D. Awschalom, R. A. Buhrman, J. M. Daughton, S. von Molnar, M. L. Roukes, A. Y. Chtchelkanova, and D. M. Treger, *Science* **294**, 1488 (2001).

²H. Ohno, *Science* **281**, 951 (1998).

³U. von Essen and W. Klemm, *Z. Anorg. Allg. Chem.* **317**, 25 (1962).

⁴R. Didenko and F. P. Gortsema, *J. Phys. Chem. Solids* **24**, 863 (1963).

⁵A. Svane, Z. Szotek, W. M. Temmerman, and H. Winter, *Solid State Commun.* **102**, 473 (1997).

⁶V. Kanchana, G. Vaitheeswaran, X. X. Zhang, Y. M. Ma, A. Svane, and O. Eriksson, *Phys. Rev. B* **84**, 205135 (2011).

⁷R. P. C. Schram, J. G. Boshoven, E. H. P. Cordfunke, R. J. M. Konings, and R. R. van der Laan, *J. Alloys Compd.* **252**, 20 (1997).

⁸A. Rukmangad, M. Aynyas, and S. P. Sanyal, *Indian J. Pure Appl. Phys.* **47**, 114 (2009).

⁹J. Staun Olsena, J.-E. Jørgensen, L. Gerward, G. Vaitheeswaran, V. Kanchana, and A. Svane, *J. Alloys Compd.* **533**, 29 (2012).

¹⁰H. Cynn, M. Lipp, W. Evans, and Y. Ohishi, *J. Phys.: Conf. Ser.* **215**, 012010 (2010).

¹¹S. B. Schneider, D. Baumann, A. Salamat, and W. Schnick, *J. Appl. Phys.* **111**, 093503 (2012).

¹²Y. C. Wang, J. Lv, L. Zhu, and M. Y. Ma, *Phys. Rev. B* **82**, 094116 (2010).

¹³Y. C. Wang, J. Lv, L. Zhu, and Y. M. Ma, *Comput. Phys. Commun.* **183**, 2063 (2012).

¹⁴P. E. Blöchl, *Phys. Rev. B* **50**, 17953 (1994).

¹⁵G. Kresse and J. Furthmüller, *Phys. Rev. B* **54**, 11169 (1996).

¹⁶H. J. Monkhorst and J. D. Pack, *Phys. Rev. B* **13**, 5188 (1976).

¹⁷S. L. Dudarev, G. A. Botton, S. Y. Savrasov, C. J. Humphreys, and A. P. Sutton, *Phys. Rev. B* **57**, 1505 (1998).

¹⁸S. L. Dudarev, M. R. Castell, G. A. Botton, S. Y. Savrasov, C. Muggelberg, G. A. D. Briggs, A. P. Sutton, and D. T. Goddard, *Micron* **31**, 363 (2000).

¹⁹P. Larson, W. R. L. Lambrecht, A. Chantis, and M. van Schilfhaarde, *Phys. Rev. B* **75**, 045114 (2007).

²⁰M. A. Blanco, E. Francisco, and V. Luana, *Comput. Phys. Commun.* **158**, 57 (2004).

²¹A. Togo, F. Oba, and I. Tanaka, *Phys. Rev. B* **78**, 134106 (2008).

²²A. Iandelli and E. Botti, *Accad. Naz. Lincei Conveg. Lincei* **25**, 129 (1937).

²³J. M. Jakobsen, G. K. H. Madsen, J.-E. Jørgensen, J. S. Olsen, and L. Gerward, *Solid State Commun.* **121**, 447 (2002).

²⁴F. Birch, *Phys. Rev.* **71**, 809 (1947).

²⁵G. L. Olcese, *J. Phys. F: Met. Phys.* **9**, 569 (1979).

²⁶J. Danan, C. de Novion, and R. Lallemand, *Solid State Commun.* **7**, 1103 (1969).

²⁷I. Barin, *Thermochemical Data of Pure Substances* (VCH, New York, 1987).

²⁸G. V. Sin'ko and N. A. Smirnov, *J. Phys.: Condens. Matter* **14**, 6989 (2002).

²⁹B. B. Karki, G. J. Ackland, and J. Crain, *J. Phys.: Condens. Matter* **9**, 8579 (1997).

³⁰J. Wang, S. Yip, S. R. Phillpot, and D. Wolf, *Phys. Rev. B* **52**, 12627 (1995).

³¹Z. W. Li, Y. Xu, G. Y. Gao, T. Cui, and Y. M. Ma, *Phys. Rev. B* **79**, 193201 (2009).

³²Y. Li, Y. M. Ma, T. Cui, Y. Yan, and G. T. Zou, *Appl. Phys. Lett.* **92**, 101907 (2008).

³³L. J. Zhang, Y. Wang, T. Cui, Y. W. Li, Y. Li, Z. He, Y. M. Ma, and G. T. Zou, *Phys. Rev. B* **75**, 144109 (2007).

³⁴J. S. Tse, S. Desgreniers, Y. Ohishi, and T. Matsuoka, *Sci. Rep.* **2**, 372 (2012).